materials

MDPI

Article

Nondestructive Monitoring Hydration of Belite Calcium Sulfoaluminate Cement by EIS Measurement

Lin Chi [1], Mian Wang [1], Zhuolin Wang [2], Zhenming Li [3,*], Bin Peng [1,*] and Junjie Li [1]

[1] School of Environment and Architecture, University of Shanghai for Science and Technology, Shanghai 200093, China; chilin@usst.edu.cn (L.C.); 213382216@st.usst.edu.cn (M.W.); 1935023313@st.usst.edu.cn (J.L.)
[2] Shanghai Key Laboratory of Engineering Structure Safety, Shanghai Research Institute of Building Sciences Co., Ltd., Shanghai 200032, China; wzllzw@163.com
[3] Microlab, Faculty of Civil Engineering and Geoscience, Delft University of Technology, 2628 CN Delft, The Netherlands
* Correspondence: z.li-2@tudelft.nl (Z.L.); BinPeng@usst.edu.cn (B.P.)

Abstract: In this study, the impact of water-to-cement (w/c) ratios of belite calcium sulfoaluminate cement (BCSA) on the hydration kinetics and the electrochemical impedance spectroscopy (EIS) parameters is studied. According to the analysis of classic hydration measurements, such as calorimetry tests, chemical shrinkage content, and chemically bound water content, it can be concluded that a higher w/c ratio clearly accelerates the hydration of BCSA cement paste. The electrical resistivity of BCSA0.35 cement paste is more than 4.5 times that of BCSA0.45 and BCSA0.5, due to the gradually densified micropore structure blocking the electrical signal transmission rather than the free charged-ion content. The porosity of BCSA0.5 is 27.5% higher than that of BCSA0.35 and 7.8% higher than that of BCSA0.45, which proves the resistivity is clearly related to the variation in microstructure, especially for the porosity and pore size distribution. The novelty of this study is the linear regression with logarithm terms of electrical resistivity and classic hydration parameters such as chemical shrinkage, cumulative hydration heat, and chemically bound water is established to extend the classical expression of cement hydration degree. It indicates that the electrochemical impedance spectroscopy can be taken as a nondestructive testing measurement to real-time monitor the cement hydration process of cement-based materials.

Keywords: belite calcium sulfoaluminate cement; resistivity; cement hydration; EIS measurement

Citation: Chi, L.; Wang, M.; Wang, Z.; Li, Z.; Peng, B.; Li, J. Nondestructive Monitoring Hydration of Belite Calcium Sulfoaluminate Cement by EIS Measurement. *Materials* **2022**, *15*, 4433. https://doi.org/10.3390/ma15134433

Academic Editor: Gwenn Le Saout

Received: 1 June 2022
Accepted: 21 June 2022
Published: 23 June 2022

1. Introduction

As the primary binder material in the construction industry, cement is produced and consumed dramatically, especially in developing countries [1,2]. The cement industry is upgrading to produce new types of cement to reduce CO_2 emissions and energy consumption to improve resource utilization [3–6]. Belite calcium sulfoaluminate (BCSA) cement is composed of belite, calcium sulfoaluminate, ferrite, and calcium sulfate [3,7]. As the main phase in BCSA cement, C2S has a lower firing temperature in the kiln (typically around 1250 °C), which decreases CO_2 emissions by 12–15% compared with ordinary Portland cement [8,9].

Compared with OPC cement, the hydration process of the BCSA cement system is slightly different. As the basic mineral composition, calcium sulfoaluminate reacted with calcium sulfate and forms ettringite and aluminum hydroxide, which provides the early age mechanical strength for the cement matrix. When calcium sulfoaluminate is almost consumed, the monosulphoaluminate is formed. C-S-H gel and portlandite are the major hydration products of C2S, which provide long-age mechanical strength and better durability for cementitious materials [10–12].

In the last few years, nondestructive testing measurements (NDT), such as dynamic or vibration tests, acoustic emission techniques, infrared image methods, and ultrasonic methods have been applied to assess the damage and infernal defects of civil engineering structures [13–20]. The optimization of concrete detection technology effectively improves the accuracy of detection and reduces the quality of concrete problems aroused by the building safety hazards, promoting the improvement of the quality of construction projects. As one of the NDT methods, the electrochemical impedance spectroscopy (EIS) test is considered an effective test method to analyze the early performance of cement-based materials [21–25].

Microstructure analysis, such as X-ray diffraction (XRD), scanning electron microscopy (SEM), hydration heat analysis, and thermogravimetric analysis (TGA), is commonly used to study the early hydration characteristics of cement-based materials [26,27]. However, except for hydration heat analysis, these testing methods can only capture the hydration characteristics of cement-based materials at a certain moment, which cannot monitor the early hydration process of cement-based materials in real-time without damage, and it is difficult to accurately predict and evaluate the mechanical strength and durability of cement-based materials at a later stage. Based on the EIS method, real-time monitoring of early hydration performance of cement-based materials and the microstructure variation prediction can be solved. However, few studies focus on the hydration assessment by the EIS measurement of cement-based materials, especially for the BCSA cement system [28].

According to our previous studies [29,30], the microstructure development of the BCSA cement-based material system can be characterized by the EIS method. A modified linear equation involving resistivity, chemical shrinkage, chemically bonded water, and hydration heat release is proposed. However, that study was only focused on cement paste with various additives, with the influence of w/c ratios unclarified. The aim of this work is to clarify the impact of the w/c ratio on the hydration kinetics and the electrochemical performance of the BCSA cement paste. The novelty of this study is the potential correlations between traditional hydration parameters, such as chemical shrinkage, chemically bound water, hydration heat, and electrical resistivity.

2. Materials and Methods

2.1. Materials

BCSA cement was produced by Tianjin Cement Co., Ltd. The chemical compositions of BCSA cement obtained by X-ray fluorescence spectrometry (XRF, PW4400, Panalytical Inc.) are shown in Table 1. The Blaine fineness and absolute density of BCSA cement is 3700 cm^2/kg and 3.10 g/cm^3, respectively. Three w/c ratios (0.34, 0.45 and 0.5) are applied for BCSA cement paste.

Table 1. Chemical composition of BCSA cement (wt.%).

SiO_2	CaO	Fe_2O_3	Al_2O_3	Na_2O	K_2O	MgO	SO_3	LOI
14.16	49.6	2.69	21.65	0.13	0.25	0.96	9.54	1.02

2.2. Hydration Heat

The hydration heat of BCSA cement pastes was detected by a TAMAIR isothermal calorimeter at the temperature of 21 °C. With the distilled water injected into the vessel, the paste was inner-mixed for 180 s in the calorimetry bottle. Isothermal calorimetry test was monitoring the kinetics of cement hydration in the first 72 h.

2.3. Chemical Shrinkage

According to ASTM C 1608-12, the chemical shrinkage content of BCSA cement paste was measured [31]. In total, 10 g cement paste was filled in a 20 ml vial (ϕ 27.5 mm, H 57 mm) and vibrated for 30 s on a vibrating table. Distilled water was filled in the remaining space of the vial. A rubber stopper with a 1 ml capillary tube embedded was

set at top of the vial. The paraffin oil was instilled in the capillary tube in case of water evaporation. The whole set was transferred into a water bath at 21 ± 1 °C. The waterline of the capillary tubes was recorded at 15 min as the starting line and once a day for 28 d. For each ratio, the chemical shrinkage of three samples was measured for average.

2.4. Chemically Bound Water

Freshly mixed cement paste was cast in 2 cm × 2 cm × 2 cm mold, demolded after 24 h and cured in the climate chamber with 65% RH, 21 °C until further testing. The degree of hydration of each binder was tested on days 1, 3, 7, and 28, respectively.

Cement paste was smashed to 3 mm grains and stopped hydration by the acetone-methanol mixtures. In the BCSA cement system, samples were dried in a vacuum drying chamber at 50 °C instead of 105 °C in the case of ettringite transformation. Then, the samples were calcined at 1050 °C in the furnace for 1 h. According to Powers' model [32], chemically bound water at a certain age can be calculated by the following equation:

$$m_{chem} = \frac{m_{50} - m_{1050}}{m_{50}} \times 100\% \quad (1)$$

where m_{50} or m_{1050} is the cement mass after drying at 105 °C or 1050 °C.

2.5. Compressive Strength

Samples with the dimension of 20 mm× 20 mm × 20 mm were cast and demolded after 24 h, then cured in the curing room with 21 ± 1 °C and RH > 65%. The compressive strength of BCSA cement paste was measured with the loading rate of 2400 N/s ± 200 N/s on days 3, 7, and 28 according to ASTM C 109/109M-21 [33].

2.6. Pore Size Distribution

The pore structure of BCSA cement samples was measured on day 28 by Mercury intrusion porosimetry (MIP). MIP was measured by Micromeritics AutoPore IV9500 (Micromeritics Instrument Corporation) with a contact angle of 140° at 25 °C. The maximum and minimum pressures were set at 414 MPa and 1.4 kPa, respectively. The samples were cut into 5 mm cubes and stopped the cement hydration by the acetone-solvent exchange for 12 h.

2.7. EIS Measurement

Fresh mixed BCSA cement pastes were cast in the acrylic molds (65 mm × 30 mm × 47 mm) [34]. Two stainless steel-welded meshes (47 mm × 47 mm) with a distance of 40 mm were served as electrodes and embedded into BCSA cement paste. The experimental setup of EIS measurement of the BCSA cement paste is present in Figure 1. The EIS experiment was measured by an electrochemical workstation (VersaSTAT 4000 A Princeton). The frequency is set at 10^5–0.1 Hz and the amplitude is set at 10–100 mV [35]. The measurement was taken during different hydration periods (1–12 h, 1–28 d). ZsimpWin 3.5 (Echem Software) is integrated with the VersaStudio software (Princeton Applied Research) to analyze Nyquist and Bode diagrams.

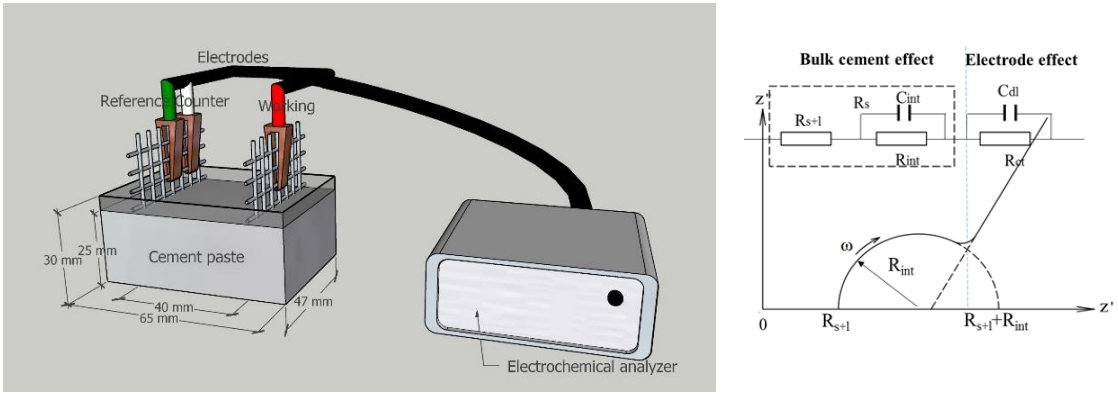

Figure 1. Experimental setup of EIS measurement of the BCSA cement paste and the equivalent circuit model [29].

3. Results

3.1. Hydration Heat Release

Figure 2 shows the hydration heat release of BCSA cement paste with various w/c ratios. The initial heat release is corresponding to the dissolution heat. The induction stage at around 4.5 h is considered a nucleation and growth process. A sharp exothermic peak was followed and characterized to be the acceleration of ettringite formation. The acceleration stage continues until the sulfate ions in the solution were consumed [30,36]. It is observed that the main exothermic peak became stronger in BCSA0.5 (in Figure 2a). For the cumulative heat release (Figure 2b), the effect of w/c showed similar trends on BCSA cement pastes. The hydration rate of BCSA0.35 is relatively low. Certain water content is needed for the formation of hydration products. With a relatively higher amount of water, the less the nuclear site is and hydrates cannot grow larger to cover the spatial gap between each particle and form the microstructure of the cement matrix.

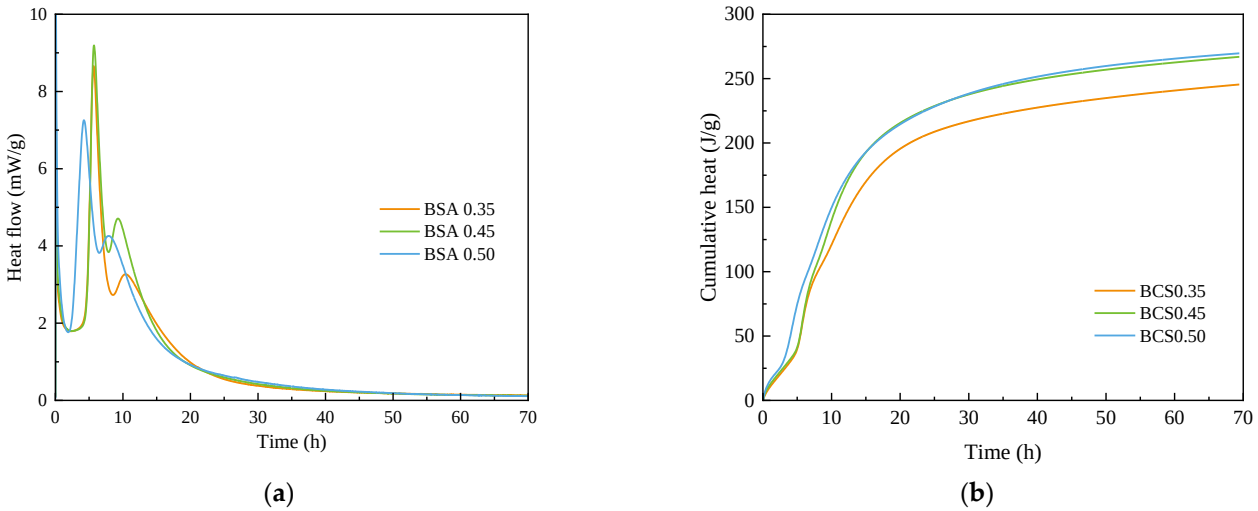

Figure 2. Heat flow (**a**) and cumulative heat curves (**b**) of BCSA cement pastes within 72 h.

3.2. Chemically Bound Water

Isothermal calorimetry measurement is mainly applied to investigate the early hydration kinetics of BCSA cement paste and chemically bound is applied to evaluate the hydration kinetics for the long age [30]. The chemically bound water contents of BCSA cement paste at days 1–28 are shown in Figure 3. The chemically bound water content of all BCSA pastes distinctly increases at days 1–3 and then stabilizes at days 3–28. It is due to a relatively higher hydration rate of the ye'elimite phase at an early age and a low hydration

rate of C_2S at days 3–28. The chemically bound water of BCSA0.5 is relatively higher than BCSA0.35 or 0.45, which is consistent with the calorimetry results.

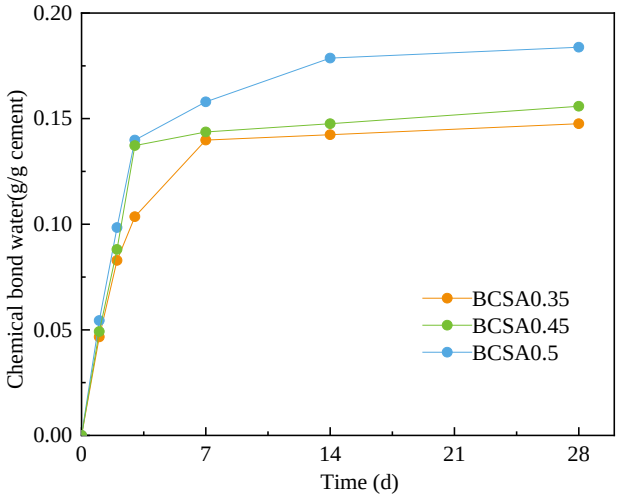

Figure 3. Chemically bound water content of BCSA cement pastes at days 1–28.

3.3. Chemical Shrinkage

The chemical shrinkage content of BCSA cement pastes with different w/c ratios at the age of 1 d–28 d is shown in Figure 4. There is little difference in chemical shrinkage behavior of BCSA pastes with different w/c ratios at 0–5 h. The chemical shrinkage content of BCSA0.5 is slightly higher than that of BCSA0.35 and BCSA0.45 at days 1–10. After day 10, the chemical shrinkage content of all binders tends to be stable at around 0.10 mL/g. For an open water system, the chemical shrinkage content of BCSA pastes of different w/c ratios is hard to measure. Considering the applicability of the three test methods discussed above, the EIS technique is applied to monitor and characterize the whole hydration stage of cement [37–39].

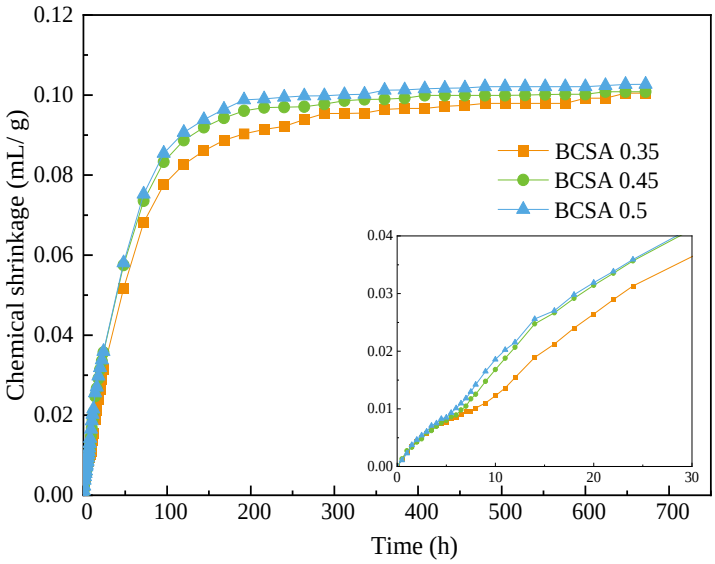

Figure 4. Chemical shrinkage of BCSA pastes with different w/c ratios.

3.4. Compressive Strength

Figure 5 presents the compressive strength of BCSA paste with different w/c ratios. It is obvious that the compressive strength of BCSA cement paste increases with the curing age and decreases with the w/c ratios. The compressive strength of BCSA0.35 at 3 d is increased by 158.4% than that of BCSA0.45 and 167.0% than that of BCA0.5. The compressive strength

of BCSA0.35 at 28 d is increased by 18.6% than that of BCSA0.45 and 132.5% than that of BCA0.5. In general, the w/c ratio has a strong effect on the compressive strength of BCSA cement paste, especially at the early age of 3 d.

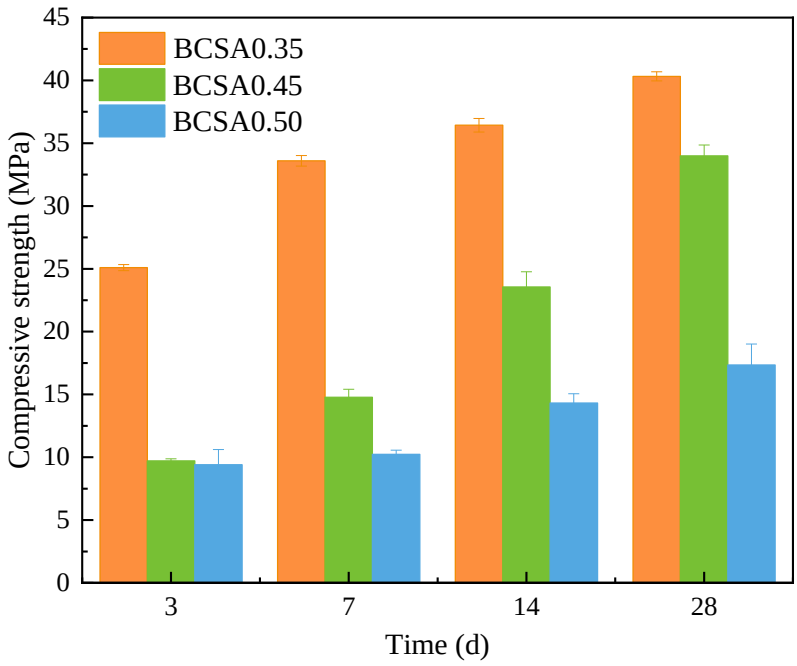

Figure 5. Compressive strength of BCSA pastes with different w/c ratios.

3.5. EIS Measurement

Nyquist and Bode curves and fitting curves of BCSA0.35, 0.45 and 0.50 at 1 d, 3 d, 7 d, 14 d, and 28 d are present in Figure 6. The radius of the high-frequency arc increases with hydration age [29,40]. The equivalent circuit model R_{s+l} ($R_{int}C_{int}$) ($R_{ct}C_{dl}$) is applied to analyze the impedance spectrum [41]. According to the above equivalent circuit, R_{s+l} and R_{int} can be extracted [15,42,43]. Compared with R_{int}, C_{int} is several orders of magnitude lower and is not counted. Therefore, as the total value of R_{s+l} and R_{int}, R_s is taken as an important parameter to evaluate the hydration reaction and transport properties of the BCSA cement paste [17,44]. Electrochemical parameters of equivalent circuit R {CR} {CR} in Nyquist curves Figure 6 are presented in Appendix A.

The electrical resistivity of BCSA cement pastes with various w/c ratios at days 1–14 and day 28 is shown in Figure 7. The resistivity of BCSA cement paste increases corresponding to the curing age. The electrical resistivity curve of all samples is basically the same in the first 24 h and the charge transfer only depends on the electrons in the pore solution [45]. After 24 h, the electrical resistivity of all samples decreases with increasing w/c ratio. With the microstructural growth and the accumulation of hydration products, the porosity and pore connectivity become lower [46]. Additionally, the gradually densified the micropore structure block electrical signal transmission [16]. These variations in the microstructure of cement-based materials can be expressed in terms of resistivity; therefore, the EIS measurement is a simple but efficient method to characterize the microstructure variation [47].

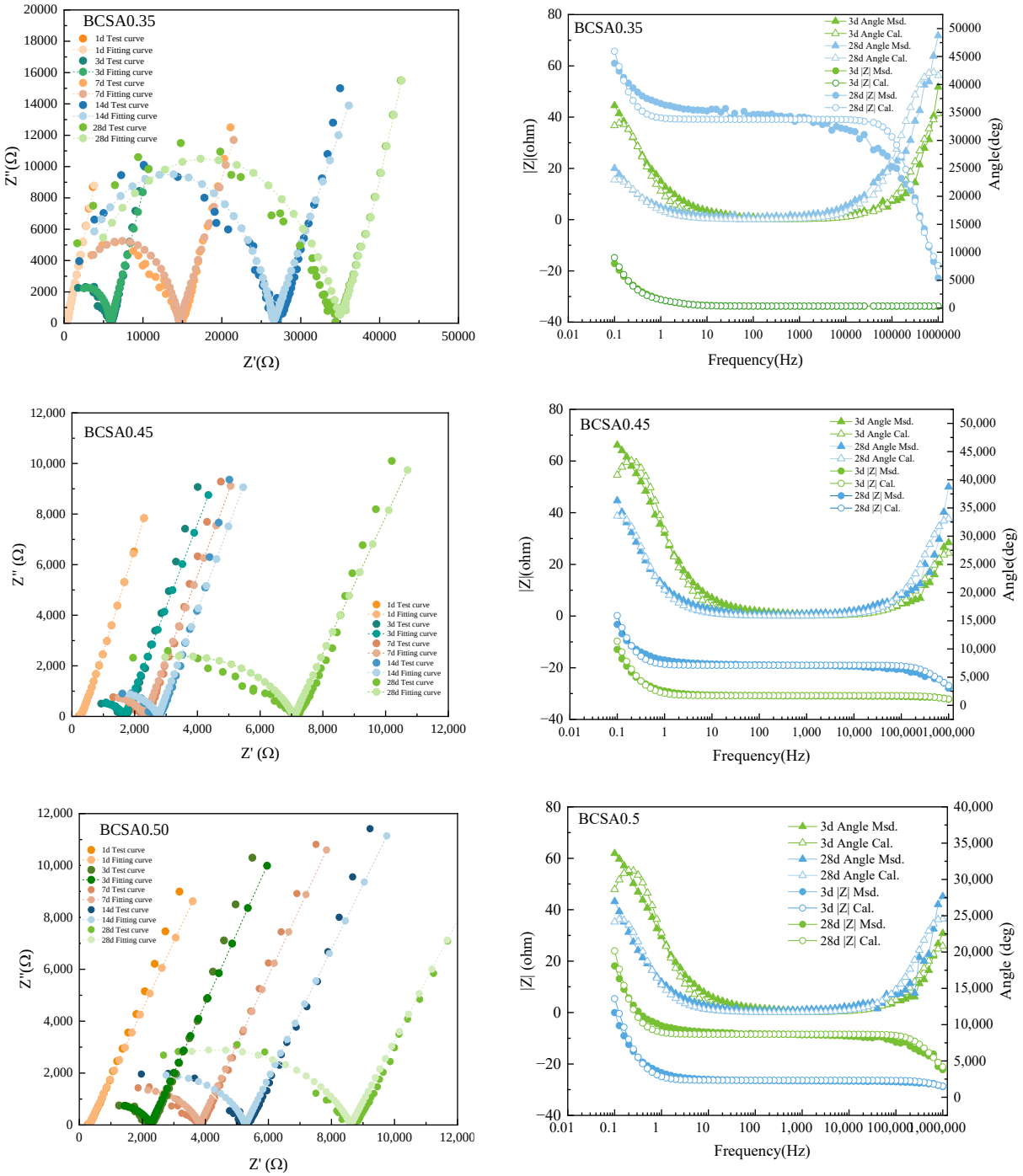

Figure 6. Nyquist and Bode curves and fitting curves of BCSA0.35, 0.45 and 0.50 at 1 d, 3 d, 7 d, 14 d, and 28 d.

3.6. Porosity Measurement

The pore structure and pore size distribution of cement paste BCSA0.35, BCSA0.45 and BCSA0.50 are measured by MIP measurement are shown in Table 2 and Figure 8. The porosity of BCSA0.5 is 27.5% higher than that of BCSA0.35 and 7.8% higher than that of BCSA0.45.

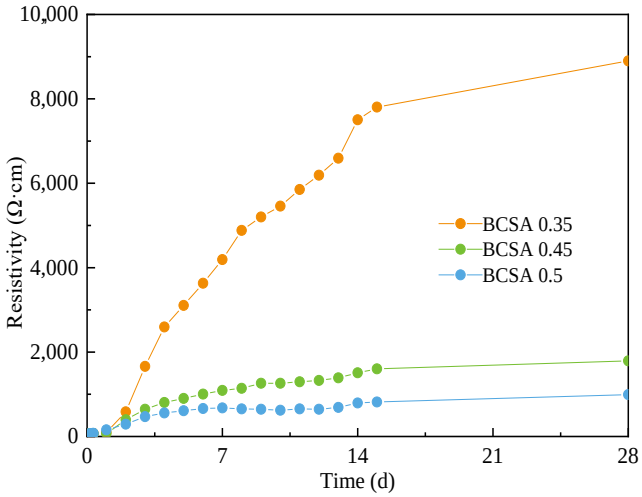

Figure 7. The electrical resistivity of BCSA cement pastes with various w/c ratio.

Table 2. Porosity and tortuosity of BCSA cement pastes.

	BCSA0.35	BCSA0.45	BCSA0.50
Porosity	38.01	44.94	48.45
Tortuosity	88.61	63.82	51.59

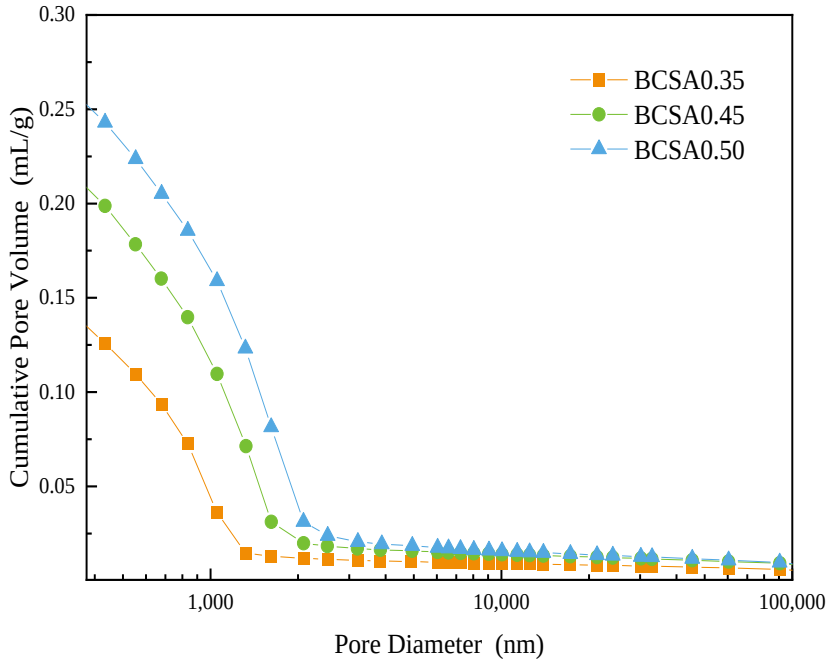

Figure 8. Pore size distribution of BCSA cement pastes with various w/c ratios at 28 d.

Since the conductivity of solid and vapor phases are several orders of magnitude lower than the liquid phase [48–50], it is assumed that the electrical conduction in the cement matrix only occurs through its liquid phases. Therefore, ion concentration in the liquid phase and tortuosity of cement microstructure are two key factors affecting the electrical resistivity of the cement system, which can be expressed by Equation (2) [51].

$$\rho_t = \beta^{-1}\phi^{-1}\rho_0 \quad (2)$$

where ρ_0 is the resistivity of the liquid phase, ρ_t is the electrical resistivity of the bulk cement paste, ϕ is the total porosity of liquid-filled pores, and β is the pore connectivity and is equal to the inverse of tortuosity.

With hydration products constantly fill the microstructure in the cement matrix, a continuous decrease in the total porosity is observed. The variation in the pore structure of BCSA cement paste is consistent with that of resistivity, which proves that resistivity can reflect the porosity, the average pore size, and the ion concentration of the pore solution during the cement hydration process.

4. Discussions

4.1. Correlations between Electrical Resistivity and Hydration Heat Release

Figure 9 presents the relation curve of the hydration heat release and electrical resistivity of BCSA cement pastes with various w/c ratios. The linear fitting curve and the correlation equation of the total heat release from hydration heat and the resistivity are established in Equation (3). The correlation coefficient is close to 1. The relationship between volume resistivity and cumulative heat release of the BCSA cement paste can be induction as Equation (4). This result indicates that resistivity extracted from the EIS test can be regarded as a real-time monitoring parameter and applied to measure the hydration heat of mass concrete structures in the future.

$$\begin{gathered} Q\,(\mathrm{t}) = 71.43\,\ln\rho_{0.35}(\mathrm{t}) - 427.64\;R^2 = 0.988 \\ Q\,(\mathrm{t}) = 90.91\,\ln\rho_{0.45}(\mathrm{t}) - 547.45\;R^2 = 0.996 \\ Q\,(\mathrm{t}) = 113.63\,\ln\rho_{0.50}(\mathrm{t}) - 694.20\;R^2 = 0.996 \end{gathered} \tag{3}$$

$$\begin{gathered} Q\,(\mathrm{t}) = f_1(r)\,\ln\rho_r\,(\mathrm{t}) + f_2(r) \\ f_1(r) = 268.97\,r - 24.56\;R^2 = 0.946 \\ f_2(r) = 1694.4\,r - 177.79\;R^2 = 0.940 \end{gathered} \tag{4}$$

where ρ_r (t) is the electrical resistivity at a certain time, in Ω cm; Q (t) is the cumulative hydration heat at time t, in J/g; r is the w/c ratio; and $f_1(r)$ and $f_2(r)$ are the slope and intercept, respectively, and are the functions of the w/c ratio.

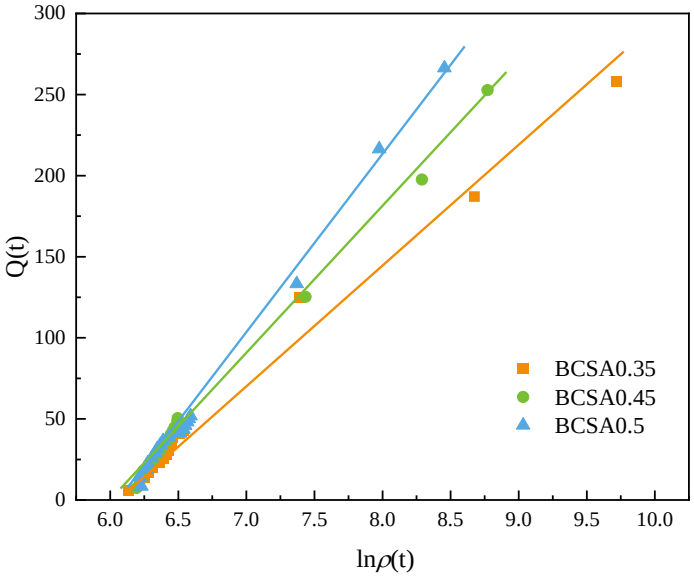

Figure 9. Correlation between cumulative hydration heat and electrical resistivity of BCSA pastes with various w/c ratios.

4.2. Correlations between Electrical Resistivity and Chemical Shrinkage

Linear correlations between chemical shrinkage and the logarithm of the electrical resistivity of BCSA pastes with various w/c ratios are present, see Figure 10. By further induction, the relationship equation between bulk electrical resistivity and chemical shrinkage of hardened BCSA cement pastes can be obtained, as shown in Equation (6). With the increase in the w/c ratio, the slope and intercept of the characteristic function increase correspondingly and have a good linear relationship with the w/c ratio. Therefore, the corresponding chemical shrinkage content of cement-based materials can be obtained by monitoring the resistivity variation.

$$Cs\ (t) = 0.02\ \ln\rho_{0.35}(t) - 0.12\ R^2 = 0.999$$

$$Cs\ (t) = 0.03\ \ln\rho_{0.45}(t) - 0.18\ R^2 = 0.997$$

$$Cs\ (t) = 0.04\ \ln\rho_{0.5}\ (t) - 0.22\ R^2 = 0.992 \quad (5)$$

$$Cs\ (t) = f_3(r)\ \ln\rho_r\ (t) + f_4(r)\ (6)$$

$$f_3(r) = 0.129\ r - 0.026\ R^2 = 0.964$$

$$f_4(r) = 0.657\ r - 0.111\ R^2 = 0.994 \quad (6)$$

where Cs (t) is the chemical shrinkage content of BCSA cement paste at a certain time, in mL/g; and $f_3(r)$ and $f_4(r)$ are the slope and intercept, respectively, and are the functions of the w/c ratio.

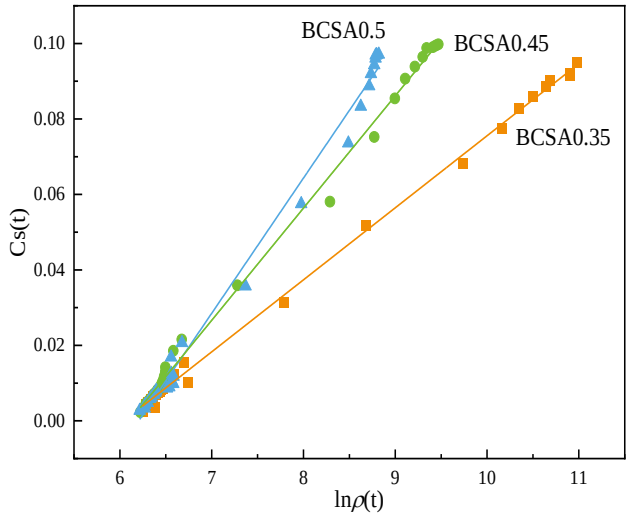

Figure 10. Correlation between chemical shrinkage content and electrical resistivity of BCSA pastes with various w/c ratios.

4.3. Correlations between Electrical Resistivity and Chemically Bound Water

The linear relationship between the logarithm of resistivity and the chemically bound water of the BCSA cement pastes with different w/c ratios is shown in Figure 11. By further induction, the relationship equation between bulk electrical resistivity and chemically bound water of hardened BCSA cement pastes can be obtained, as shown in Equation (8).

$$Cw\ (t) = 0.02\ \ln\rho_{0.35}(t) - 0.12\ R^2 = 0.980$$

$$Cw\ (t) = 0.04\ \ln\rho_{0.45}(t) - 0.21\ R^2 = 0.949$$

$$Cw\ (t) = 0.06\ \ln\rho_{0.5}\ (t) - 0.42\ R^2 = 0.959 \quad (7)$$

$$Cw\ (t) = f_5(r)\ \ln\rho_r\ (t) + f_6(r)$$

$$f_5(r) = 0.257\ r - 0.071\ R^2 = 0.964$$

$$f_6(r) = 1.843\ r - 0.549\ R^2 = 0.840 \quad (8)$$

where Cw (t) is the chemically bound water content of cement paste at a certain time, in mL/g; m_1 and m_2 are the fitting parameters; and $f_5(r)$ and $f_6(r)$ are the slope and intercept, respectively, and are the functions of the w/c ratio.

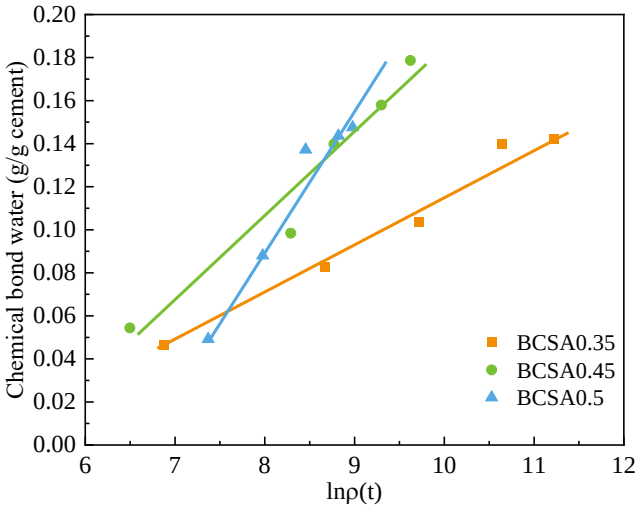

Figure 11. Correlation between chemically bound water and electrical resistivity of BCSA pastes with various w/c ratios.

4.4. Hydration Degree Evaluation

The chemical shrinkage content, cumulative heat release content, and chemically bound water content are all important parameters that characterize the degree of cement hydration. Additionally, the relationship between Lnρ(t) and $Q(t)$, $Cs(t)$, or $CW(t)$ (Equations (4), (6), and (8)) belongs to linear regression with logarithmic terms and can be deduced as Equation (9).

$$\alpha = \frac{Q_n(t)}{Q_n^0} = \frac{CW(t)}{CW^0} = \frac{CS(t)}{CS^0} = \frac{Ln\rho(t)}{Ln\rho^0} \quad (9)$$

where $Q(t)$ or Q_n^0 is the cumulative hydration heat at time t or full hydration, in J/g; $CW(t)$ or CW^0 is the chemically bound water content of cement paste at a certain time or full hydration, in mL/g; $CS(t)$ or CS^0 is the chemical shrinkage content of cement paste at a certain time or full hydration, in mL/g; and $\rho(t)$ or $Ln\rho^0$ is the electrical resistivity at a certain time or full hydration, in Ω cm.

Based on the variation in electrical resistivity or electrical impedance, electrochemical impedance spectroscopy measurement can be applied to characterize the microstructure evolution of cement-based materials in the early hydration stage. Additionally, the real-time monitoring properties of cement-based materials can be obtained by establishing the correlation between resistivity and major physical and chemical performance parameters. Additionally, EIS measurement can enhance the accuracy of the hydration prediction model of belite calcium sulfoaluminate cement, especially for the early hydration age.

5. Conclusions

Electrical impedance spectroscopy was applied to monitor the hydration of belite calcium sofoaluminate cement with a w/c ratio of 0.35, 0.45, and 0.50. Additionally, the main conclusions are summarized as follows.

(1) Higher w/c ratios clearly accelerate the hydration of BCSA cement paste. The porosity of BCSA0.5 is 27.5% higher than that of BCSA0.35 and 7.8% higher than that of BCSA0.45.

(2) The electrical resistivity of BCSA0.35 cement paste is more than 4.5 times that of BCSA0.45 and BCSA0.5, due to gradually densified the micropore structure blocking the electrical signal transmission rather than the free charged-ion content. The resistivity is clearly related to the variation in the microstructure, especially for the porosity and pore size distribution during the hydration process.
(3) Linear regression with logarithmic terms of electrical resistivity and classic hydration parameters, such as chemical shrinkage, cumulative hydration heat, and chemically bound water, is built to express the cement hydration degree.

Author Contributions: Conceptualization, L.C.; Data curation, L.C., Z.W. and B.P.; Formal analysis, M.W. and J.L.; Funding acquisition, L.C., Z.W. and B.P.; Methodology, L.C.; Project administration, Z.L. and Z.W.; Resources, M.W. and J.L.; Software, Z.W.; Validation, M.W. and Z.L.; Writing–review & editing, L.C. All authors have read and agreed to the published version of the manuscript.

Funding: The authors would like to appreciate the financial support by the Shanghai Sailing Program No. 20YF1431800, Key Laboratory of Performance Evolution and Control for Engineering Structures (Tongji University), the Ministry of Education (No. 2019KF-5), and the Open Fund of Shanghai Key Laboratory of Engineering Structure Safety (No. 2019-KF07).

Institutional Review Board Statement: Not applicable.

Informed Consent Statement: Not applicable.

Data Availability Statement: Not applicable.

Conflicts of Interest: The authors declare no conflict of interest. This article does not contain any studies with human participants or animals performed by any of the authors. Informed consent was obtained from all individual participants included in the study.

Appendix A

Table A1. Electrochemical parameters of an equivalent circuit R{CR}{CR} in Nyquist curves Figure 6.

w/c	Age	R_1(ohm)	CPE_1(F)	R_2(ohm)	CPE_2(F)	R_3(ohm)
0.35	1 d	367.4	1.379×10^{-4}	672.3	9.489×10^{-5}	2.433×10^{4}
	3 d	1169	1.042×10^{-4}	4857	5.659×10^{-11}	1.893×10^{4}
	7 d	2145	8.163×10^{-5}	1.255×10^{4}	3.684×10^{-11}	2.125×10^{4}
	14 d	3475	6.324×10^{-5}	2.329×10^{4}	3.277×10^{-11}	2.413×10^{4}
	28 d	2874	5.949×10^{-5}	3.090×10^{4}	2.401×10^{-11}	2.491×10^{4}
0.45	1 d	265.4	1.654×10^{-4}	326.5	1.244×10^{-4}	2.718×10^{4}
	3 d	720.7	1.347×10^{-4}	1011	2.408×10^{-10}	2.253×10^{4}
	7 d	969.5	1.332×10^{-4}	1412	1.633×10^{-10}	2.401×10^{4}
	14 d	1110	1.358×10^{-4}	1704	1.173×10^{-10}	2.438×10^{4}
	28 d	1718	1.245×10^{-4}	5387	5.965×10^{-11}	2.399×10^{4}
0.55	1 d	323.2	8.808×10^{-5}	524.6	1.382×10^{-4}	2.701×10^{4}
	3 d	913.6	1.090×10^{-4}	1419	1.628×10^{-10}	2.174×10^{4}
	7 d	1211	1.061×10^{-4}	2687	8.599×10^{-11}	2.323×10^{4}
	14 d	1730	1.012×10^{-4}	3622	7.698×10^{-11}	2.403×10^{4}
	28 d	2202	9.444×10^{-5}	6469	5.248×10^{-11}	2.517×10^{4}

References

1. Schneider, M. The Cement Industry On the Way to a Low-Carbon Future. *Cem. Concr. Res.* **2019**, *124*, 105792. [CrossRef]
2. Scrivener, K.L.; John, V.M.; Gartner, E.M. Eco-Efficient Cements: Potential Economically Viable Solutions for a low-CO_2 Cement-Based Materials Industry. *Cem. Concr. Res.* **2018**, *114*, 2–26. [CrossRef]
3. Julphunthong, P. Synthesizing of Calcium Sulfoaluminate-Belite (CSAB) Cements From Industrial Waste Materials. *Mater. Today Proc.* **2018**, *5 Pt 1*, 14933–14938. [CrossRef]
4. Borštnar, M.; Daneu, N.; Dolenec, S. Phase Development and Hydration Kinetics of Belite-Calcium Sulfoaluminate Cements at Different Curing Temperatures. *Ceram. Int.* **2020**, *46*, 29421–29428. [CrossRef]

5. Popescu, C.D.; Muntean, M.; Sharp, J.H. Industrial Trial Production of Low Energy Belite Cement. *Cem. Concr. Comp.* **2003**, *25*, 689–693. [CrossRef]
6. Wang, D.; Noguchi, T.; Nozaki, T.; Higo, Y. Investigation On the Fast Carbon Dioxide Sequestration Speed of Cement-Based Materials at 300 °C–700 °C. *Constr. Build. Mater.* **2021**, *291*, 123392. [CrossRef]
7. Dolenec, S.; Šter, K.; Borštnar, M.; Nagode, K.; Ipavec, A.; Žibret, L. Effect of the Cooling Regime on the Mineralogy and Reactivity of Belite-Sulfoaluminate Clinkers. *Minerals* **2020**, *10*, 910. [CrossRef]
8. Stanek, T.; Sulovsky, P. Active Low-Energy Belite Cement. *Cem. Concr. Res.* **2015**, *68*, 203–210. [CrossRef]
9. Rungchet, A.; Chindaprasirt, P.; Wansom, S.; Pimraksa, K. Hydrothermal Synthesis of Calcium Sulfoaluminate-Belite Cement From Industrial Waste Materials. *J. Clean. Prod.* **2016**, *115*, 273–283. [CrossRef]
10. Martín-Sedeño, M.C.; Cuberos, A.J.M.; De la Torre, Á.G.; Álvarez-Pinazo, G.; Ordónez, L.M.; Gateshki, M.; Aranda, M.A.G. Aluminum-Rich Belite Sulfoaluminate Cements: Clinkering and Early Age Hydration. *Cem. Concr. Res.* **2010**, *40*, 359–369. [CrossRef]
11. Morin, V.; Termkhajornkit, P.; Huet, B.; Pham, G. Impact of Quantity of Anhydrite, Water to Binder Ratio, Fineness On Kinetics and Phase Assemblage of Belite-Ye'elimite-Ferrite Cement. *Cem. Concr. Res.* **2017**, *99*, 8–17. [CrossRef]
12. Winnefeld, F.; Martin, L.H.J.; Müller, C.J.; Lothenbach, B. Using Gypsum to Control Hydration Kinetics of CSA Cements. *Constr. Build. Mater.* **2017**, *155*, 154–163. [CrossRef]
13. Jiang, S.; Zhou, D.; Zhang, L.; Ouyang, J.; Yu, X.; Cui, X.; Han, B. Comparison of Compressive Strength and Electrical Resistivity of Cementitious Composites with Different Nano- and Micro-Fillers. *Arch. Civ. Mech. Eng.* **2018**, *18*, 60–68. [CrossRef]
14. Li, W.; Li, X.; Chen, S.J.; Liu, Y.M.; Duan, W.H.; Shah, S.P. Effects of Graphene Oxide On Early-Age Hydration and Electrical Resistivity of Portland Cement Paste. *Constr. Build. Mater.* **2017**, *136*, 506–514. [CrossRef]
15. Yim, H.J.; Lee, H.; Kim, J.H. Evaluation of of Mortar Setting Time by Using Electrical Resistivity Measurements. *Constr. Build. Mater.* **2017**, *146*, 679–686. [CrossRef]
16. Farzanian, K.; Pimenta Teixeira, K.; Perdigão Rocha, I.; De Sa Carneiro, L.; Ghahremaninezhad, A. The Mechanical Strength, Degree of Hydration, and Electrical Resistivity of Cement Pastes Modified with Superabsorbent Polymers. *Constr. Build. Mater.* **2016**, *109*, 156–165. [CrossRef]
17. Wei, X.; Xiao, L. Kinetics Parameters of Cement Hydration by Electrical Resistivity Measurement and Calorimetry. *Adv. Cem. Res.* **2014**, *26*, 187–193. [CrossRef]
18. Fu, C.; Huang, J.; Dong, Z.; Yan, W.; Gu, X. Experimental and Numerical Study of an Electromagnetic Sensor for Non-Destructive Evaluation of Steel Corrosion in Concrete. *Sens. Actuators A Phys.* **2020**, *315*, 112371. [CrossRef]
19. Bolborea, B.; Baera, C.; Dan, S. Concrete Compressive Strength by Means of Ultrasonic Pulse Velocity and Moduli of Elasticity. *Materials* **2021**, *14*, 7018. [CrossRef]
20. Breysse, D.; Martínez-Fernández, J.L. Assessing Concrete Strength with Rebound Hammer: Review of Key Issues and Ideas for More Reliable Conclusions. *Mater. Struct.* **2014**, *47*, 1589–1604. [CrossRef]
21. Martín-del-Rio, J.J.; Canivell, J.; Falcón, R.M. The Use of Non-Destructive Testing to Evaluate the Compressive Strength of a Lime-Stabilised Rammed-Earth Wall: Rebound Index and Ultrasonic Pulse Velocity. *Constr. Build. Mater.* **2020**, *242*, 118060. [CrossRef]
22. Pucinotti, R. Reinforced Concrete Structure: Non Destructive in Situ Strength Assessment of Concrete. *Constr. Build. Mater.* **2015**, *75*, 331–341. [CrossRef]
23. Dwivedi, S.K.; Vishwakarma, M.; Soni, P.A. Advances and Researches On Non Destructive Testing: A Review. *Mater. Today Proc.* **2018**, *5 Pt 1*, 3690–3698. [CrossRef]
24. Da Silva, G.F.; Martini, S.; Moraes, J.C.B.; Teles, L.K. AC Impedance Spectroscopy (AC-IS) Analysis to Characterize the Effect of Nanomaterials in Cement-Based Mortars. *Constr. Build. Mater.* **2021**, *269*, 121260. [CrossRef]
25. Hu, X.; Shi, C.; Liu, X.; Zhang, J.; de Schutter, G. A Review On Microstructural Characterization of Cement-Based Materials by AC Impedance Spectroscopy. *Cem. Concr. Compos.* **2019**, *100*, 1–14. [CrossRef]
26. Shakir Abbood, I.; Weli, S.S.; Hamid, F.L. Cement-Based Materials for Self-Sensing and Structural Damage Advance Warning Alert by Electrical Resistivity. *Mater. Today Proc.* **2021**, *46*, 615–620. [CrossRef]
27. Da Silveira, G.D.; de Carvalho, L.M.; Montoya, N.; Domenech-Carbó, A. Evaluation of Aging Processes of Petroleum Asphalt Cements by Solid State Electrochemical Monitoring. *Electrochim. Acta* **2018**, *270*, 461–470. [CrossRef]
28. Sun, C.; Zhang, J.; Yan, C.; Yin, L.; Wang, X.; Liu, S. Hydration Characteristics of Low Carbon Cementitious Materials with Multiple Solid Wastes. *Constr. Build. Mater.* **2022**, *322*, 126366. [CrossRef]
29. Chi, L.; Wang, Z.; Lu, S.; Zhao, D.; Yao, Y. Development of Mathematical Models for Predicting the Compressive Strength and Hydration Process Using the EIS Impedance of Cementitious Materials. *Constr. Build. Mater.* **2019**, *208*, 659–668. [CrossRef]
30. Chi, L.; Li, W.; Li, Z.; Wang, Z.; Lu, S.; Liu, Q. Investigation of the Hydration Properties of Cement with EDTA by Alternative Current Impedance Spectroscopy. *Cem. Concr. Compos.* **2022**, *126*, 104365. [CrossRef]
31. *ASTM C 1608-17*; Standard Test Method for Chemical Shrinkage of Hydraulic Cement Paste. American Society for Testing and Materials. ASTM International: West Conshohocken, PA, USA, 2017.
32. Powers, D.R.; Brace, R.A. Fetal Cardiovascular and Fluid Responses to Maternal Volume Loading with Lactated Ringer Or Hypotonic Solution. *Am. J. Obstet. Gynecol.* **1991**, *165*, 1504–1515. [CrossRef]

33. *ASTM C109/C109M-21*; Standard Test Method for Compressive Strength of Hydraulic Cement Mortars (Using 2-In. Or [50mm] Cube Specimens). ASTM International: West Conshohocken, PA, USA, 2021.
34. *ASTM C1702-17*; Standard Test Method for Measurement of Heat of Hydration of Hydraulic Cementitious Materials Using Isothermal Conduction Calorimetry. ASTM International: West Conshohocken, PA, USA, 2017.
35. Dong, Z.; Torbati-Sarraf, H.; Hussein, H.Z.; Poursaee, A. Harmonic Analysis On the Effect of Potential Perturbations and Electrodes Arrangements On the Electrochemical Impedance (EIS) Measurement of Cementitious Material. *Constr. Build. Mater.* **2021**, *273*, 121701. [CrossRef]
36. Tambara, L.U.D.; Cheriaf, M.; Rocha, J.C.; Palomo, A.; Fernández-Jiménez, A. Effect of Alkalis Content On Calcium Sulfoaluminate (CSA) Cement Hydration. *Cem. Concr. Res.* **2020**, *128*, 105953. [CrossRef]
37. Madej, D.; Kruk, A. Monitoring Hydration of Sr-doped Calcium Zirconium Aluminate (Ca, Sr)7ZrAl6O18 Cement Via Electrochemical Impedance Spectroscopy (EIS) and Supported Techniques. *Constr. Build. Mater.* **2019**, *206*, 307–320. [CrossRef]
38. Hay, R.; Li, L.; Celik, K. Shrinkage, Hydration, and Strength Development of Limestone Calcined Clay Cement (LC3) with Different Sulfation Levels. *Cem. Concr. Compos.* **2022**, *127*, 104403. [CrossRef]
39. Wang, L.; Jin, M.; Wu, Y.; Zhou, Y.; Tang, S. Hydration, Shrinkage, Pore Structure and Fractal Dimension of Silica Fume Modified Low Heat Portland Cement-Based Materials. *Constr. Build. Mater.* **2021**, *272*, 121952. [CrossRef]
40. Burduhos-Nergis, D.; Vizureanu, P.; Sandu, A.V.; Bejinariu, C. Evaluation of the Corrosion Resistance of Phosphate Coatings Deposited on the Surface of the Carbon Steel Used for Carabiners Manufacturing. *Appl. Sci.* **2020**, *10*, 2753. [CrossRef]
41. Gu, P.; Xie, P.; Beaudoin, J.J.; Brousseau, R.A.C. Impedance Spectroscopy (I): A New Equivalent Circuit Model for Hydrated Portland Cement Paste. *Cem. Concr. Res.* **1992**, *22*, 833–840. [CrossRef]
42. Tang, S.W.; Cai, X.H.; He, Z.; Zhou, W.; Shao, H.Y.; Li, Z.J.; Wu, T.; Chen, E. The Review of Early Hydration of Cement-Based Materials by Electrical Methods. *Constr. Build. Mater.* **2017**, *146*, 15–29. [CrossRef]
43. Dong, B.; Zhang, J.; Wang, Y.; Fang, G.; Liu, Y.; Xing, F. Evolutionary Trace for Early Hydration of Cement Paste Using Electrical Resistivity Method. *Constr. Build. Mater.* **2016**, *119*, 16–20. [CrossRef]
44. Liao, Y.; Wei, X. Relationship between Chemical Shrinkage and Electrical Resistivity for Cement Pastes at Early Age. *J. Mater. Civ. Eng.* **2014**, *26*, 384–387. [CrossRef]
45. Dong, W.; Li, W.; Tao, Z.; Wang, K. Piezoresistive Properties of Cement-Based Sensors: Review and Perspective. *Constr. Build. Mater.* **2019**, *203*, 146–163. [CrossRef]
46. Wu, Y.; Duan, P.; Yan, C. Role of Layered Double Hydroxides in Setting, Hydration Degree, Microstructure and Compressive Strength of Cement Paste. *Appl. Clay Sci.* **2018**, *158*, 123–131. [CrossRef]
47. He, H.; Zhu, Y.; Zhou, A. Electrochemical Impedance Spectroscopy (EIS) Used to Evaluate Influence of Different External Pressures, Curing Ages and Self-Healing Environments On the Self-Healing Behavior of Engineered Cementitious Composites (ECC). *Constr. Build. Mater.* **2018**, *188*, 153–160. [CrossRef]
48. Sanish, K.B.; Neithalath, N.; Santhanam, M. Monitoring the Evolution of Material Structure in Cement Pastes and Concretes Using Electrical Property Measurements. *Constr. Build. Mater.* **2013**, *49*, 288–297. [CrossRef]
49. Tang, S.W.; Cai, X.H.; He, Z.; Zhou, W.; Shao, H.Y.; Li, Z.J.; Wu, T.; Chen, E. The Review of Pore Structure Evaluation in Cementitious Materials by Electrical Methods. *Constr. Build. Mater.* **2016**, *117*, 273–284. [CrossRef]
50. Klaver, J.; Hemes, S.; Houben, M.; Desbois, G.; Radi, Z.; Urai, J.L. The Connectivity of Pore Space in Mudstones: Insights From High-Pressure Wood's Metal Injection, BIB-SEM Imaging, and Mercury Intrusion Porosimetry. *Geofluids* **2015**, *15*, 577–591. [CrossRef]
51. Rajabipour, F.; Weiss, J. Electrical Conductivity of Drying Cement Paste. *Mater. Struct.* **2007**, *40*, 1143–1160. [CrossRef]